

Techniques for the Study of the Electronic Properties

Marcos Fernández-García¹, José A. Rodríguez²

¹Instituto de Catálisis y Petroleoquímica CSIC, 28049 Madrid, SPAIN

²Brookhaven National Laboratory, Upton, NY 11973, USA

To be published in "Synthesis, Properties and Applications of Oxide Nanomaterials"

June 2006

Chemistry Department

Brookhaven National Laboratory

P.O. Box 5000

Upton, NY 11973-5000

www.bnl.gov

Notice: This manuscript has been authored by employees of Brookhaven Science Associates, LLC under Contract No. DE-AC02-98CH10886 with the U.S. Department of Energy. The publisher by accepting the manuscript for publication acknowledges that the United States Government retains a non-exclusive, paid-up, irrevocable, world-wide license to publish or reproduce the published form of this manuscript, or allow others to do so, for United States Government purposes.

This preprint is intended for publication in a journal or proceedings. Since changes may be made before publication, it may not be cited or reproduced without the author's permission.

DISCLAIMER

This report was prepared as an account of work sponsored by an agency of the United States Government. Neither the United States Government nor any agency thereof, nor any of their employees, nor any of their contractors, subcontractors, or their employees, makes any warranty, express or implied, or assumes any legal liability or responsibility for the accuracy, completeness, or any third party's use or the results of such use of any information, apparatus, product, or process disclosed, or represents that its use would not infringe privately owned rights. Reference herein to any specific commercial product, process, or service by trade name, trademark, manufacturer, or otherwise, does not necessarily constitute or imply its endorsement, recommendation, or favoring by the United States Government or any agency thereof or its contractors or subcontractors. The views and opinions of authors expressed herein do not necessarily state or reflect those of the United States Government or any agency thereof.

Chapter 6

Techniques for the Study of the Electronic Properties

Marcos Fernández-García
Instituto de Catálisis y Petroleoquímica
CSIC, Campus Cantoblanco
28049 Madrid, Spain

José A. Rodríguez
Chemistry Department
Brookhaven National Laboratory
Upton, NY 11973, USA

Table of contents:

- 6.1 Introduction
- 6.2 XANES
- 6.3 Optical absorption
- 6.4 Photoemission spectroscopy
- References

6.1 Introduction

The electronic structure of a solid is affected by size and altered from the continuous electronic levels forming a band, characteristic of bulk or micro-sized solids, to discrete-like or quantized levels. This is drastically observed when the particle size goes down to the nano-meter range and is the origin of the so-called “quantum confinement” terminology referring to this phenomenon. From a solid state point of view, electronic states of confined materials can be considered as being a superposition of bulk-like states with a concomitant increase of the oscillator strength.¹ The valence/conduction band-width and position observables of a solid oxide are functions of the crystal potential and this, in turn, is perturbed by effect of the size in two ways; a short-range effect induced by the presence of ions with a different coordination number and bond distance, and a large-range one, induced by changes in the Madelung potential of the oxide. Theoretical analyses for oxides show a redistribution of charge when going from large periodic structures to small clusters which is roughly considered small for ionic solids and significantly important for covalent ones.^{2,3} Chapter 1 of this book describes the most recent theoretical frameworks employed to deal with these physical phenomena while here we will describe their influence in physico-chemical observables obtained by spectroscopical techniques.

In brief, natural consequences of these size-induced complex phenomena are band narrowing and change of band energy.^{1,4} The thermodynamic limit (at 0 K) for a chemical step/reaction that can be carried out with charged particles (electron or holes located in electronic levels) is given by the position of the band edges, the so-called flat band potential. Both size-induced band-related changes modulate the onset energy where absorption occurs, e.g., the band gap energy, changing also the Fermi level of the system and the chemical potential of charge carrier species hosted by these electronic

levels. An additional consequence of nanostructure when speaking of semiconductor or insulator oxides is the presence of new electronic states located in the bulk band gap. As well known, perfect crystals do not display such electronic features and are thus directly or indirectly related to a finite size in the nano-meter range. Such mid gap states are sometimes called “surface states” as the main structural sources of their origin are the presence of a different local symmetry at the surface and/or the presence of additional defects, among which, the most typical in nano-oxides are of punctual nature (oxygen vacancies or interstitial ions) located at/near the surface.^{3,5,6} The energy distribution of vacancy-related mid gap energy levels have been experimentally obtained,^{7,8,9} allowing the comparison between different samples. Roughly speaking, donor levels are energetically near the conduction band while acceptor ones are located near the valence band and create gaussian-like distributions with a width proportional to the 2/3 power of the number of defects.¹⁰ Such electronic levels display distributions ranging from 0 to a few tens (ca. 0.7) of eV from the corresponding flat band potential with maxima (or depths) located sometimes at 0-100 meV^{7,11} and others well above such energies.^{3,10,12} Both types are phenomenologically differentiated in shallow and deep (mid-gap) electronic levels and display distinctive features when charged particles (electrons or holes) interact with them.¹³ One last general point to mention here is the absence in nano-particulate materials of band bending under contact with the external media in a heterogeneous chemical reaction.¹⁴ This infers an important property to all nano-structured oxides under light excitation, as it facilitates the presence of both charge carrier species, electron and holes, at the surface of the particle, ready to be involved in subsequent chemical steps. This contrasts with the situation of bulk-like semiconductors where one of the charge carriers is typically depleted from the surface area.

These electronic implications of size are mainly studied by using three different techniques based on the interaction between photons and the solid phase. The first one uses (soft and hard) X-ray photons to excite internal or core electrons and analyze the absorption coefficient as a function of the incident photon energy; this is the so called X-ray absorption near edge structure (XANES) which allows the scanning of the (locally projected, see below) density of unoccupied electronic states. A second type of technique is based on optical absorption of visible/ultraviolet photons with an energy that allows to study intra-atomic (typically d-d transitions in transition elements) and charge transfer (near or band gap energies) excitations; they are frequently utilized to study (optical) band gap energies and unoccupied localized states at the band gap of nano-meter solids. A third type of technique, photoemission, is used to analyze the density of occupied states of solids and may give information about the valence band as well as more inner levels. Several emission optical techniques may also provide information about the electronic properties of solid oxides but usually they do not add additional input to the main electronic characteristics as studied by the three techniques above mentioned. A main problem when dealing with nanoparticulated solid oxides, which is present in all the results obtained with these spectroscopical techniques, comes from the broad size distribution typically obtained during the synthesis of the material, significantly larger than those characteristic of other types of materials. This obscures the detailed investigation of the electronic properties in a large number of occasions.

6.2 XANES

As already discussed in Chapter 5 for XAS techniques, XANES spectroscopy probes the electronic state of an absorbent atom of the X-ray radiation. The two XAS techniques are sensible to local order, making them specially suitable for analyzing

nanostructured materials, but differ in the fact that XANES is essentially not affected by thermal effects; in absence of vibronic or specific (non-frequent) cases of spin-orbit coupling, the recording temperature does not affect the XANES shape.^{15,16,17,18} Recent work on XANES concerning nanostructured oxides has been published for Al,¹⁹ Mg,²⁰ Ti,^{21,22,23,24,25} V,²⁶ Fe,^{27,28,29} Ni,³⁰ Zn,³¹ Sn-In³² and Ce^{33,34,35,36,37} containing systems while older work is summarized in refs. 18 and 38. These studies showed that bulk XANES shape is typically reached by clusters of around 80-100 atoms and, thus, solids with a typical dimension below 4 nm show a characteristic, distinctive XANES shape. This happens because, in terms of the scattering theory, the different continuum resonances (CRs) are dominated by contributions corresponding to different coordination shells and may not be present or display variations in energy/intensity with respect to the bulk material in the corresponding XANES spectrum of a size-limited material.^{19,21,28,29,30} At the moment, not precise information is available concerning differences between surface species present in nanostructured and 2D-infinite surfaces. A general feature shared by all nanostructured oxide materials with size typically below 10-15 nm is that they display broader CRs with respect to well-crystallized references.^{19,21,24,25,26,31,33,39} This can be observed in the inset of Figure 6.1; the derivative spectra give evidence of a larger overlap between CRs. The reason for this can be understood in terms of the f-rule.⁴⁰ This rule implies that the total absorption over all edges and energies is a constant independent of the final state nature; therefore, disorder, inherent to nanostructured materials, broadens the spectrum without altering the overall intensity.²² The large overlap of CRs usually limits information concerning electronic effects of nanostructure but some details are still available/resolved when analyzed low energy (below 1 KeV) absorption edges, even for nearly amorphous materials.^{41,42}

A strong influence of size can be also found in the $1s \rightarrow d$ pre-edge transition present at K absorption edges ($1s$ absorption spectra, see Figure 6.1a) of transition metal cations inserted in an oxide matrix. Other elements do not present this pre-edge as they have a fully occupied d band. Both a direct $1s$ to nd quadrupole transition and dipole transitions to states with $(n+1)p$ character hybridized with the nd sub-band are possible.¹⁸ Typically, the matrix element of a dipole transition (see equation 5.3.2 in Chapter 5) is about two orders of magnitude larger than quadrupole ones but, on the other hand, the amount of d character at or immediately below of the Fermi region is by far larger than the p one in transition metal ions. Depending on the particular system we are dealing with, the contributions from dipole and quadrupole can be equivalent or one can be neglected. In particular, for centro-symmetric systems, like cubic systems, only a very small admixture of p states is allowed into the nd sub-band while in non-centro-symmetric systems p/d mixing is symmetry allowed. It is rather obvious that corners, edges and, in general, surface positions are non-centro-symmetric and can be therefore differentiated in the case of many oxides.

The $1s \rightarrow d$ transition can be composed by several peaks, depending of the symmetry and oxidation state of the metal ion constituting the oxide. Reviews of the literature can be found in refs. 18 and 43. The electronic fine details enclosed in the pre-edge structure are however masked by resolution problems when working with most of the ions of chemical interest (transition or lanthanides) but the recent setting-up of resonant inelastic X-ray scattering may soon eliminate such problem while working with hard X-rays which allow to characterize the system in essentially any experimental condition (e.g. in-situ).⁴⁴ In the first transition row, with current set-ups three/two peaks can be observed from Ti to Fe cations in centro-symmetric positions due to the $(s)p-d$ mixing of the absorbent/central cation orbitals as well as to the presence of quadrupole

transitions to d-like states of neighboring atoms. For some low oxidation states, low spin configurations and non-centro-symmetric positions of the above mentioned cations as well as from Co to Cu-containing oxides a single (most often dominant but not unique as is accompanied by shoulders) peak is obtained. As an example, Figure 6.1a displays the presence of a characteristic peak at the left of the vertical line, indicative of fivefold-coordinated surface Ti ions, not present in the bulk of the material which, therefore, allows to investigate the characteristics as well as the quantity of surface species in Titania. Data on the second and third transition row is more scarce and usually less well defined due to poor energy resolution coming from the large core-hole life-time inherent to the high photon energy used (above 17 KeV).¹⁸ As mentioned above, this may change in the near future with the removal of the life-time broadening in XANES spectra by standardizing detection schemes using low-medium energy X-ray photoemission, emission decay or Auger channels.^{44,45} Of course, this will be able to give larger resolution in the complete XANES spectrum, enhancing the electronic information extracted by using this technique but at the expense of a strong decrease in signal intensity. On the other hand, a detection scheme based in X-ray emission, like, for example, using the 1snp fluorescence channel, would open a window to site-selective XANES and the corresponding speciation of species by chemical, surface/bulk or other interesting properties.⁴⁴

XANES can be used for the characterization of oxide nanoparticles under reaction conditions, varying pressure or temperature as a function of time.^{3,18} This is illustrated by the Ce L_{III}-edge XANES data shown in Figure 2. This figure compares spectra from a Ce_{0.8}Cu_{0.2}O₂ nanocatalyst under the water gas shift (WGS) reaction ($\text{CO} + \text{H}_2\text{O} \rightarrow \text{CO}_2 + \text{H}_2$) at different temperatures.³⁷ As mentioned above, the Ce L_{III}-edge is frequently used as a “fingerprint” to characterize the electronic properties of ceria-

based materials.¹⁸ The electronic transitions behind these XANES features are complex. In pure stoichiometric CeO₂, the Ce L_{III}-edge exhibits two clear peaks frequently labeled B1 and C.¹⁸ A third peak, with lower photon energy than B1, can be obtained by curve fitting.¹⁸ Included in Figure 2 is the spectrum for a Ce(NO₃)₃•6H₂O reference, in which the cerium atoms are trivalent (Ce³⁺). The two main peaks in the spectrum of the Ce_{0.8}Cu_{0.2}O₂ sample at room temperature are separated by approximately 7eV, in agreement with results for pure CeO₂ nanoparticles.³⁷ Based on a comparison of the intensities of the spectra near the Ce³⁺ position, one is able to confirm that oxygen vacancies and Ce³⁺ cations are formed during the WGS reaction. The amount of oxygen vacancies and Ce³⁺ is seen to increase with the raise of the reaction temperature up to 300°C, but decreased at higher temperatures, especially above 400°C. This type of information is essential for establishing the mechanism of the chemical reaction and studying the behavior of the Ce_{0.8}Cu_{0.2}O₂ nanoparticles as catalysts.³⁷ In many technological applications (catalysts, sorbents, sensors, fuel cells, etc), the electronic properties of oxide nanoparticles undergo important changes during operation and XANES can be a very useful technique to follow these changes *in-situ*.^{15,18,37,41}

6.3 Optical Absorption

Optical techniques can be devoted to the analysis of metal oxide electronic structures. As a major part of oxides are semiconductors or insulators we will first detail such cases. The absorbance $\alpha(\lambda)$ of a solid semiconductor can be calculated by using the relation:

$$T = \frac{(1-F)^2 \exp^{-\alpha(\lambda)\delta}}{1-F^2 \exp^{-2\alpha(\lambda)\delta}} \quad (6.3.1)$$

Where T is the measured transmittance, F the reflectance, and δ is the optical path length.⁴⁶ Metal oxides can be direct or indirect semiconductors depending on whether the valence to conduction band electronic transition is dipole allowed or forbidden. In the later case, the electronic transition is vibrationally allowed through vibronic coupling and phonon assisted. The intensity of the corresponding electronic transition is several orders of magnitude lower for indirect with respect to direct band gap semiconductors.⁴⁷ Indirect band gap semiconductors display thus a step structure at the absorption onset originated from the momentum conserving optical phonon absorption and emission and a general stronger dependence of the absorption coefficient with energy near the edge.^{46,47} The absorption coefficient dependence of energy is stated in equation 6.3.2, where n equals $\frac{1}{2}$ or 2 for, respectively, direct and indirect semiconductors;

$$\alpha(\lambda) = B(\hbar\nu - E_g)^n (\hbar\nu)^{-1} \quad (6.3.2)$$

Where B is a constant and E_g is the band gap energy.

As mentioned in the introduction, the nanostructure has a strong impact in the electronic structure of oxides producing the so-called quantum size of confinement effects. From a solid-state point of view, nanostructured oxides have discrete, atom-like electronic levels which can be considered as being a superposition of bulk-like states with a concomitant increase in oscillator strength.^{4,48} Electronic effects related to quantum confinement potentially visible by optical absorption are the shift in band gap energy as a function of primary particle size as well as the discretization of the absorption, presenting a well-defined structure instead of the featureless profile typical of bulk solids.^{4,48} In metal oxides however the influence of nanostructure in optical

spectroscopy data is mostly confined to the absorption onset energy as inhomogeneous broadening resulting from the particle size distribution induces broadening of the spectrum and limits the study of the shape of the optical absorption spectrum.

The onset of the optical absorption spectrum occurs at the so-called first exciton (electron-hole pair created after light absorption) or optical band gap energy. The most widespread, simple theoretical framework to study the influence of confinement effects and, particularly, the primary particle size influence in exciton energy, is the so-called effective-mass approximation (EMA).^{4,48} Other theories as the free-exciton collision model (FECM)⁴⁹ have been implemented and although are much less utilized may become alternatives in the near future for massive use. The EMA theory assumes parabolic energy bands, infinite confining potential at the interface of the spherical semiconductor particle, and limits main energy terms to electron-hole interaction energy (Coulomb term) and the confinement energy of electron and hole (kinetic term). From experimental work it is customary to identify three different energy regions as a function of the average crystalline radius (R) of the semiconductor particle:

- 1) $R > a_B$, where a_B is the exciton Bohr radius of the extended/bulk semiconductor, defined as $a_B = a_e + a_h$ where a_e and a_h are the electron and hole Bohr radii, respectively. This is the regime of weak confinement and the dominant energy is the Coulomb term and there occurs a size quantization of the motion of the exciton (electron-hole pair is treated as a quasi-particle). The energy of the lowest excited state is a function of R as;

$$E(R) = E_g + \frac{\hbar^2 \pi^2}{2MR^2} \quad (6.3.3)$$

Where E_g is the band gap energy of the extended/bulk semiconductor, and M is the mass of the exciton ($M = m_e^* + m_h^*$; m^* being the effective mass of electron and hole). This indicates a blue shift of $E(R)$ as a function of R^{-2} .

2) $R < a_B$ or strong confinement region, where the Colulomb term can be treated as a perturbation and electron and holes are treated as confined independent particles, so the exciton is not formed and separate size quantization of electron and hole is the dominant factor. In this case $E(R)$ for the lowest excited state of a spherical cluster is given by:

$$E(R) = E_g + \frac{\hbar^2 \pi^2}{2R^2} \left(\frac{1}{m_e^*} + \frac{1}{m_h^*} \right) - \frac{1.786e^2}{\epsilon_2 R} + 0.248E_R \quad (6.3.4)$$

Where the first corrective term to E_g is the confinement term, the second is the Coulomb correction with ϵ_2 the dielectric constant of the bulk semiconductor, and the third is the spatial correlation energy correction, being E_R the exciton Rydberg energy.^{4,48,50} As well known at present, this formulae overestimates the $E(R)$ energy and is being corrected by using an effective bond-order model (EBOM) to construct the hole Hamiltonian, include spin-orbit coupling, and finite confining potential,⁵¹ or by introducing the effect of shape distortion from a spherical particle model.⁵² Alternative methods including these novel points in the framework of the tight-binding⁵³ or pseudopotential^{54,55} theories have been also published. An important additional challenge to all theories is to develop consistent theoretical estimates of the ϵ_2 dependence with R .⁴⁸

3) The region between weak and strong confinement has not been thoroughly investigated but has deserved some attempts for specific semiconductors.⁵⁶ The intermediate regime is precisely defined as the region where $R_e > R_B > R_h$, and here

the hole is quasi-localized and the absorption spectrum comes from the oscillation movement of the hole around the center of the nano-crystal, suffering an average potential corresponding to the much faster electron movement.⁴⁸

Form the above discussion, it can be thus concluded that metal oxide semiconductors would present, as a first rough approximation, an optical band gap energy with an inverse squared dependence of the primary particle size if quantum confinement dominates the energy behavior of the band gap. Figure 6.3 shows that this happens to be the case for (direct band gap) Fe_2O_3 ⁵⁷ or (indirect band gap) CdO ⁵⁸ but not for Cu_2O ,⁵⁹ CeO_2 ,^{36,60} ZnO ,^{61,62} and TiO_2 .^{63,64} Limited deviations from the R^{-2} behavior, as observed for ZnO in Figure 6.3 or SnO_2 ⁶⁵ can be based in the known fact that the theory (equations 6.3.3 and 6.3.4) overestimates the blue shift and can be justified with a proper calculation of electronic states by using simple quantum mechanical methods, while marked deviations are usually based in several chemical/physical phenomena not accounted for in the previous discussion. In the case of Cu_2O ⁵⁹ or CeO_2 ^{36,60,66} it appears to be directly related with the presence of Cu^{2+} (remarkably for very low particle size) and Ce^{3+} ions at the surface of the nanostructured materials. At the moment it is not clear if the presence of these oxidation states are intrinsic to the nanostructure or result from the specific procedure of preparation. The case of WO_3 share also some of the difficulties pointed out above. Kubo *et al.* were able to show that the band gap of this oxide decrease with size from ca. 3.0 to 2.8 eV as a function of R^{-1} ,⁶⁷ but the presence of a variable number of oxygen defects, reduced W redox states and mid-gap electronic states with size makes this an open question.⁶⁸ Besides electronic modifications, alien ions, like Cu^{2+} and Ce^{3+} above, induce strain effects and concomitant structural differences in atomic positions with respect to bulk positions. The influence of strain in the absorption spectrum has been

nicely demonstrated in the work of Ong et al. for ZnO,⁶⁹ showing the splitting of the first exciton peak for large values of compressive strain. Strain effects are inherent to nanostructured materials^{3,70} and may be comprised in the general, ambiguous term of “surface” effects usually claimed to account for significant deviations from equations 6.3.3 and 6.3.4. Surface effects related to the preparation method and particularly important for very low particle size are sometimes observed for certain oxides, as SnO₂⁷¹ or ZrO₂.⁷²

TiO₂ is the other example included in Fig. 6.3 having a band gap energy behavior with marked differences from that expected from equations 6.3.3 and 6.3.4. While bulk TiO₂ is an indirect semiconductor, nanostructured TiO₂ materials are likely direct ones.^{63,73} This may be a general result. As discussed in ref. 74, the confinement of charge carriers in a limited space causes their wavefunctions to spread out in momentum space, in turn increasing the likelihood of radiative transitions for bulk indirect semiconductors. This may also be the case of NiO.⁷⁵ The indirect nature of the absorption onset would complicate the analysis of the optical band gap energy due to the above mentioned step structure of the absorption onset (which includes phonon-related absorption/emission features).⁷⁶ In spite of this, the steady behavior shown in Fig. 6.3 can not be accounted for by small variations in the absorption onset and should be grounded in other physical phenomena. For small primary particle sizes, below 3-4 nm, this has been claimed to be based on a fortuitous cancellation effect between the Kinetic/Confinement and Coulomb terms in eq. 6.3.4, but electronic grounds for this phenomenon still need to be understood. For indirect band gap semiconductors, recent theoretical results⁵⁴ suggest the presence of a red shift instead of a blue one with a primary particle size decrease but recent careful experimental data corroborate the existence of the blue shift qualitatively described by eq. 6.3.4.⁷⁶

The nanostructure not only affects the band gap energy but at the long wavelength of the charge transfer or main absorption band, a weak exponential absorbance decay can be observed. At a given temperature, this region can be modeled following the Urbach empirical formulae, yielding an Energy parameter describing the width of this exponential absorption edge.⁷⁷ In certain oxides, the width of Urbach tails has been correlated with the degree of crystallinity, giving thus a quantitative tool to compare this properties on structurally similar samples.⁷⁸

As happens with the absorption, the emission spectrum followed by photoluminescence or fluorescence from nanostructured samples has specific characteristics with respect to bulk systems.^{4,48} However, they do not usually add further insights into the main electronic structure of metal oxides and will not be treated here. A last word in this section can be said concerning semi-metallic or metallic metal oxides (as VO₂ at T > 373 K). Although a metal to insulator transition is expected as a function of size,^{1,4} this has not been analyzed in detail. Therefore, as a rough picture, we may expect the discretization of electronic levels and presence of well-defined transitions, which, however, would be typically broadened by the “size distribution” effect.

6.4 Valence and Core Level Photoemission

The roots of core and valence level photoemission can be traced back to the famous article of Einstein explaining the photoelectric effect.⁷⁹ For a solid, the relationship between the kinetic energy of the photoemitted electron (E_k) and the energy of the incident radiation ($h\omega$) is given by the equation:

$$E_k = h\omega - E_B - WF \quad (6.4.1)$$

where E_B is the binding energy of the electron in the solid and WF is the system “work function” (a catch-all term whose precise value depends on both the sample and spectrometer).⁸⁰ The previous equation assumes that the photoemission process is an elastic process between matter and the external electric field. The photoemission process is the dominant de-excitation channel for atoms with atomic number Z lower than 30/50 for K/L edges, while Auger electrons dominate de-excitation for $Z > 30/50$. Thus each characteristic excitation energy ($h\omega$) will give rise to a series of photoelectron peaks which reflect the discrete binding energies of the electrons (with energy lower or equal than the excitation one) present in the system.⁸⁰ The intensity of the peak is essentially an atomic property and thus allows the quantification of the absorber atom at the surface and near surface layer.⁸⁰

In the period of 1950-1970, pioneer work by the groups of Siegbahn,⁸¹ Turner,⁸² and Spicer⁸³ showed that spectra with well resolved ionization peaks could be obtained when using high-resolution electron energy spectrometers combined with x-ray or ultraviolet radiation for photoexcitation. The typical experiments of x-ray photoelectron spectroscopy (XPS) utilize Mg $K\alpha$ (1253.6 eV) or Al $K\alpha$ (1486.6 eV) radiation to excite the electrons.⁸⁰ He I (21.21 eV) and He II (40.82 eV) are photon energies frequently used in ultraviolet photoelectron spectroscopy.⁸⁴ Synchrotrons are a very valuable tool for performing photoemission experiments.^{85,86,87} Electrons orbiting in a synchrotron emit radiation that spans a wide spectral region, is highly collimated and polarized. Using the facilities available at synchrotrons, one can get photoemission spectra that have simultaneously a very high resolution and excellent signal-to-noise ratio.^{77,78} The acquisition of spectra can be very fast, and chemical transformations can be followed as a function of time.^{88,89,90}

Valence Photoemission. Depending on their energy, the levels occupied by the electrons in a nanoparticle can be labeled as core (> 50 eV), semi-core or valence (< 20 eV).⁸⁰ In the valence region, the electrons occupy de-localized or bonding orbitals. The spectrum in this region consist of many closely spaced levels giving rise to a band structure.^{91,92,93,94} For large oxide nanoparticles, valence bands similar to those of the bulk materials are expected. As the size of the nanoparticles decreases, unique features could appear in the valence region,^{95,96} and eventually the valence bands could break down into discrete levels in the case of small oxide clusters.⁹⁷ In their bulk states, some oxides can have metallic character, but most frequently these systems behave as semiconductors or insulators and have a significant gap between the valence and conduction bands. Due to size effects, a nanoparticle could have a bandgap energy differing from that of its bulk state (see section 6.3 for a detailed analysis) and this could be detected in valence photoemission.^{96,97,98} This technique is also very useful to verify the presence of O vacancies in an oxide nanoparticle. Electronic states associated with O vacancies usually appear above the valence band of the oxide in the bandgap.^{99,100}

Core Photoemission. The discovery, during the early days of XPS,^{80,81} that non-equivalent atoms, either by symmetry or oxidation state, of the same element in a solid gave rise to core-level peaks with different binding energies had a stimulating effect in the development of the field.⁸⁰ Core-level photoemission can be very sensitive to changes in the oxidation state of an element in an oxide nanoparticle.³ Thus, different oxides of the same metal element in many cases have substantially different core level binding energies.¹⁰¹ Figure 6.4 illustrates the utility of core-level photoemission for the characterization of oxide nanoparticles. These XPS data were acquired in experiments similar to those that produced the STM images of Figure 8 in Chapter 5.¹⁰² MoO_3 and

Mo₂O₅ were prepared by the oxidation of Mo nanoparticles present on a Au(111) substrate. Initially, there is intermixing of Mo and Au. The formation of the MoO_x nanoparticles induces migration of Mo from inside the Au substrate to the surface and, thus, there is a big increase in the intensity of the signal for the Mo 3d core levels.^{102,103} A Mo → MoO₃ transformation is accompanied by a shift of ~ 4.3 eV in the Mo 3d levels. At small concentrations of molybdenum (~ 0.05 monolayer), the Mo nanoparticles can be fully oxidized (left-side panel in Figure 6.4, spectrum b). On the other hand, after oxidizing a larger concentration of molybdenum (~ 0.10 monolayer), photoemission shows a mixture of MoO₃ and Mo₂O₅ (right-side panel in Figure 6.4, spectra b, c and d).¹⁰²

Core-level binding-energy shifts constitute one of the most widely used diagnostic tools for routine chemical analysis in industrial laboratories.¹⁰⁴ A lot of effort has been focused on the interpretation of these shifts.^{80,104} A core-level binding energy is fundamentally a difference in total energy between the ground and unbound continuum excited states of a system. This difference can have initial- and final-state contributions.¹⁰⁴ To induce a core-level shift with respect to a well defined reference one can modify the initial or final state. Thus a change in the oxidation state of an element can lead to a shift in its core-level binding energies (initial state effect), but a core-level shift also can be produced by a variation in the screening of the hole left by the emitted electron (final state effect).¹⁰⁴ A priori, it is not easy to evaluate final-state contributions to core-level binding-energy shifts.^{80,104}

Several models, based on physical simplifications of the photoemission process, have been proposed for the analysis of core-level shifts in oxide compounds.^{104,105,106,107,108,109,110,111} The physical basis for a core-level shift can be illustrated by a simple charge potential model.^{80,81}

$$E_i = E_i^R + kq_i + \sum_j 3q_j/r_{ij} \quad (6.4.2)$$

where E_i is the binding energy of a particular core level on atom i , E_i^R is an energy reference, q_i is the charge on atom i , and the final term of equation (6.4.2) sums the potential at atom i due to ‘point charges’ on surroundings atoms j . The last term can be expressed as $V_i = \sum_j 3q_j/r_{ij}$. Then, the shift in binding energy for a given core level of atom i in two different chemical environments is:⁸⁰

$$E_i^{(1)} - E_i^{(2)} = k(q_i^{(1)} - q_i^{(2)}) + (V_i^{(1)} - V_i^{(2)}) \quad (6.4.3)$$

The first term, $k\Delta q_i$, indicates that an increase in binding energy accompanies a decrease in the valence electron density on atom i . The second term depends on the charge distribution of the whole system, is related to the Madelung potential of the oxide, and has an opposite sign to Δq_i in equation (6.4.3).^{80,81} For highly ionic oxides, the effects of the Madelung potential can be quite strong and dominate the overall direction of the core-level shifts.^{80,104} Thus, Hartree-Fock self-consistent field calculations for BaO clusters show that the removal of two s electrons leads to an increase of the core-level binding energies in Ba^{2+} over neutral Ba (as expected), but this increase is offset by the Madelung potential and the XPS measurements show a net negative core-level shift. The dominance of these two electrostatic effects in the core level shifts of all alkaline-earth oxides was also demonstrated.¹⁰⁶ From equation (6.4.3) it is clear that one can have a core-level shift in an oxide nanoparticle by changing the oxidation state of atom i , by modifying the Madelung potential, by the creation of O vacancies, or by just moving the atom i to a non-equivalent position (like surface ones) within the structure of the system. It is important to take into consideration that the Madelung potential of a nanoparticle or nanostructure of an oxide can be different from

that of the bulk material and affect not only the position but also the intensity of the peaks in an XPS spectrum.^{112,113}

Equation (6.4.3) is a first approximation to the problem of core level shifts, and in general should be used only in qualitative terms.^{80,104} A major simplification of the charge potential model is that it neglects relaxation effects; e.g. it does not take into account the polarization effect of the core hole on the surrounding electrons, both intra-atomic (on atom *i*) and extra-atomic (on atoms *j*).^{80,104} A precise interpretation of core-level binding energy shifts frequently requires the use of quantum-mechanical calculations.^{105,106,111} This is the best way to separate contributions from initial and final state effects.^{114,115,116} Initial state effects are frequently calculated by the Koopman's theorem which essentially depends on the "sudden approximation", explained in section 5.3, to describe the photoemission process as being realized by one electron while the remaining *N*-1 electrons of the system are "frozen". The use of the full electron (final-state) wavefunctions yields the core-hole energy. Note that several final-state wavefunctions corresponding to a localized/delocalized nature of the hole and the existence of hole-induced charge transfer ($M^{(n+1)+} - L^{-1}$) are usually possible. The latter typically produces the presence of secondary peaks, close to the main but with lower intensity, for transition metals oxides having *d* holes in the final state. The difference between these two quantities, e.g. the initial state and the core-hole energies, is the relaxation energy.^{80,104} The relaxation energy may vary from one oxide to another and with the size of the particle, since it is affected by the Madelung potential and this changes with size.^{104,113}

Charging is a phenomenon that can occur when the conductivity of the oxide nanoparticles or nanostructures is too low to replenish the photoemitted electron.^{80,104} This means that a significant net positive charge accumulates in the system, and

eventually produces a shift in the binding energy position of the core and valence levels. Unfortunately, a fully satisfactory solution to charging problems is not yet available. Several approaches have been proposed.^{80,104} A flood gun is one of the easiest and most common solutions to charging problems. It produces a huge increase in the concentration of low-energy electrons. One must verify that these “extra” electrons do not induce any structural or chemical transformation in the sample. Whenever possible, it is highly advantageous to deposit the oxide nanoparticles on a conducting support.^{117,118} During the photoemission process, electrons spill from the support and neutralize the charging effects. The data in Figure 6.4 shows how effective this approach can be.¹⁰²

The low pressure conditions in which XPS spectra are taken ($< 10^{-7}$ Torr) can induce the loss of O₂ gas and formation of O vacancies in oxide nanoparticles.¹¹² This can become a serious problem if the oxide system is easy to reduce. For example, measurements of XPS for ceria nanoparticles give a concentration of Ce³⁺ cations that is much larger than that detected with XANES.¹¹²

Acknowledgment

J.A.R. is grateful for the financial support of the US Department of Energy, Division of Chemical Sciences (DE-AC02-98CH10886 contract). M.F.G. thanks the Spanish “Ministerio de Ciencia y Tecnología” and CSIC for financial support.

References

-
- 1 Moriarty P, Rep. Prog. Phys. 64, 297 (2001).
 - 2 Noguera, C. *Physics and Chemistry at Oxide Surfaces*; Cambridge University Press: Cambridge, UK, 1996.
 - 3 Fernandez-García M., Martínez-Arias A., Hanson J.C., Rodriguez JA., Chem. Rev. 104, 4063 (2004).

-
- 4 Yoffre A, *Adv. Phys.* 42, 173 (1993).
 - 5 Al-Abadleh HA, Grassian VH, *Surf. Sci. Report.* 52, 63 (2003).
 - 6 Dietbold U, *Surf. Sci. Report.* 48, 53 (2003).
 - 7 Ikeda S, Sugiyama N, Murakami S, Kominami H, Kera Y, Noguchi H, Uosaki K, Torimoto T, Ohtani B, *Phys. Chem. Chem. Phys.* 5, 778 (2003).
 - 8 Boschloo G, Fitsmaurice D, *J. Phys. Chem. B* 103, 228 (1999).
 - 9 Durrant JR, *J. Photchem. Photobiol A* 148, 5 (2002).
 - 10 Cohen M.M, "Introduction to the quantum theory of semiconductors" (Gordon, Amsterdam, 1972).
 - 11 Durrant JR, *J. Photchem. Photobiol A* 148, 5 (2002).
 - 12 Boschloo G, Fitsmaurice D, *J. Phys. Chem. B* 103, 228 (1999).
 - 13 Mora-Seró I, Busquet J, *Nanoletters* 3, 945 (2003).
 - 14 Grätzel M, "Heterogeneous Photochemical Electron Transfer" (CRC, Boca Raton, 1989) p. 106-108.
 - 15 See "X-ray Absorption". Konigsberger, D.C.; Prins, R., Eds. Wiley, New York, 1987.
 - 16 See articles in *Chem. Rev.* 101 (2001).
 - 17 Rehr, J.J.; Albers, J.C.; *Rev. Modern Phys.* 72, 621 (2000).
 - 18 Fernández-García, M.; *Catal. Rev. Sci. Eng.* 44, 59 (2002).
 - 19 Cabaret, D.; Sainterit, P.; Idelfonse, P.; Flank, A.M.; *J. Phys. Condens. Matter* 8, 3691 (1996).
 - 20 Mozoguchi, T.; Tanaka, I.; Yoshida, M.; Oba, F.; Ogasawara, K.; Adachi, H.; *Phys. Rev. B* 2000, 61, 2180.
 - 21 Wu, Z.Y.; Ouward, G.; Gressier, P.; Natoli, C.R.; *Phys. Rev. B* 55, 10383 (1997).
 - 22 Farges, F.; Brown, G.E. Jr; Rehr, J.J.; *Phys. Rev. B* 56, 1809 (1997).
 - 23 Chen, L.X.; Rajh, T.; Wang, Z.; Thurnauer, M.C.; *J. Phys. Chem. B* 101, 10688 (1997).
 - 24 Yeung, K.L.; Maira, A.J.; Stolz, J.; Hung, E.; Hu, N.K.-C.; Wei, A.C.; Soria, J.; Chao, K.-J.; *J. Phys. Chem. B* 106, 4608 (2002).
 - 25 McCornick JR, Zhao B, Rykov S, Wang H, Chen JG, *J. Phys. Chem. B* 108, 17398 (2004).
 - 26 Sipr, O.; Simunek, A.; Bocharov, S.; Kirchner, Th.; Drager, G.; *Phys. Rev. B* 60, 14115 (1999).
 - 27 Wu, Z.Y.; Gota, S.; Jollet, F.; Pollak, M.; Gautier- Soyer, M.; Natoli, C.R.; *Phys. Rev. B* 55, 2570 (1997).
 - 28 Chen, L.X.; Liu, T.; Thurnauer, M.;Csencsits, R.; Rajh, T.; *J. Phys. Chem. B* 106, 8539 (2002).
 - 29 Wu, Z.; Xian, D.C.; Natoli, C.R.; Marcelli, A.; Paris, E.; Mollans, A.; *Appl. Phys. Lett.* 79, 1918 (2001).
 - 30 Van der Laan, G.V.; Zaanen, J.; Sawatzky, G.A.; Karnatak, R.; Estern, J.M.; *Phys. Rev. B* 33, 4253 (1986).
 - 31 Chiou JW, et al., *Appl. Phys. Lett.* 85, 3220 (2004).
 - 32 Subramanian V, Gnanasekar KI, Rambabu B, *Solid state Ionics* 175, 181 (2004).
 - 33 Nachimuthu, P.; Shih, W.-C.; Liu, R.-S.; Jang, L.-Y.; Chem., J.-M.; *J. Sol. State Chem.* 149, 408 (2000).
 - 34 Nagai, Y.; Yamamoto, T.; Tanaka, T.; Yoshida, S.; Nonaka, T.; Okamoto, T.; Suda, A.; Sugura, M.; *Catal. Today* 74, 225 (2002).
 - 35 Soldatov, A.V.; Ivanchenko, T.S.; Della Longa, S.; Kotani, A.; Iwamoto, Y.; Bianconi, A.; *Phys. Rev. B* 50, 5074 (1994).

-
- 36 Hernández-Alonso, M.D.; Hungría, A.B.; Coronado, J.M.; Martínez-Arias, A.; Conesa, J.C.; Soria, J.; Fernández-García, M.; *Phys. Chem. Chem. Phys.* 6, 3524 (2004).
- 37 Wang, X.; Rodríguez, J.A.; Hanson, J.C.; Gamarra, D.; Martínez-Arias, A.; Fernández-García, M. *J. Phys. Chem. B*, in press (2006).
- 38 Kizler, P.; *Phys. Lett. A* 172, 66 (1992).
- 39 Asuka, K.; Iwasawa, Y.; Chp. 7 in “X-ray absorption fine structure for catalysts and surfaces”; Iwasawa, Y. (Editor); World Scientific, Singapore, 1996.
- 40 Alteaelli, M.; Dexter, D.L.; Nussenzveig, H.M.; *Phys. Rev. B* 6, 4502 (1972).
- 41 Chen JG, *Surf. Sci. Rep.* 30, 1 (1997).
- 42 Sokucheyev G, et al., *Phys. Rev. B* 69, 245102 (2004).
- 43 De Groot, F.M.F.; *Chem. Rev.* 101, 1779 (2001).
- 44 De Groot FMF, et al., *J. Phys. Chem. B* 109, 20751 (2005).
- 45 Hamalainen, K.; Siddons, P.; Hastingsm, J.B.; Berman, L.E.; *Phys. Rev. Lett.* 67, 2850 (1991).
- 46 Pannkov, J.I.; *Optical Processes in Semiconductors*. Dover, New York, 1971.
- 47 Alivisatos, A.P.; *J. Phys. Chem.* 100, 13226 (1996).
- 48 Yoffe, A.D.; *Adv Phys.* 50, 1 (2001).
- 49 Glinka YD, Lin SH, Hwang LP, Chen YT, Tolk NH, *Phys. Rev. B* 64, 085421 (2001).
- 50 Bawendi, M.G.; Wilson, W.L.; Rothberg, L.; Carroll, P.J.; Jedji, T.M.; Steigerward, M.L.; Brus, L.E.; *Phys. Rev. Lett.* 65, 1623 (1990).
- 51 Laheld, V.E.H.; Einevoll, G.T.; *Phys. Rev. B* 55, 5184 (1997).
- 52 Efros, A.L.; Rosen, M.; Kuno, M.; Normal, M.; Norris, D.J.; Bawendi, M.; *Phys. Rev. B* 54, 4843 (1996).
- 53 Von Grumber, H.H.; *Phys. Rev. B* 55, 2293 (1997).
- 54 Tomasulo, A.; Ramakrisna, M.V.; *J. Chem. Phys.* 105, 3612 (1996).
- 55 Wang, L.-W.; Kim, J.; Zunger, A.; *Phys. Rev. B* 59, 5678 (1999).
- 56 Uzomi, T.; Kayanuma, Y.; Yamanaka, K.; Edamatsu, K.; Itoh, T.; *Phys. Rev. B* 59, 9826 (1999).
- 57 Iwamoto, M.; Abe, T.; Tachibana, Y.; *J. Mol. Catal. A* 55, 143 (2000).
- 58 Vigil, O.; Cruz, F.; Morales-Acabedo, A.; Contreras-Puente, G.; Vaillant, L.; Santana, G.; *Mat. Chem. Phys.* 68, 249 (2001).
- 59 Borgohain, K.; Morase, N.; Mahumani, S.; *J. Appl. Phys.* 92, 1292 (2002).
- 60 Suzuki, T.; Kosacki, I.; Petrovsky, V.; Anderson, H.U.; *J. Appl. Phys.* 91, 2308 (2001).
- 61 Viswanaha, R.; Sapra, S.; Satyani, B.; Der, B.N.; Sarma, D.D.; *J. Mat. Sci.* 14, 661 (2004).
- 62 Li L, Qui X, Li G, *J. Appl. Phys.* 87, 124101 (2005).
- 63 Serpone, N.; Lawless, D.; Khairutdinov, R.; *J. Phys. Chem.* 98, 16646 (1995).
- 64 Monticone, S.; Tufeu, R.; Kanaev, A.V.; Scolan, E.; Sánchez, C.; *Appl. Surf. Sci.* 162-163, 565 (2000).
- 65 Deng H, Hossenlopp JM, *J. Phys. Chem. B* 109, 66 (2005).
- 66 Tsunekawa, S.; Fukuda, T.; Kasuya, A.; *J. Appl. Phys.* 87, 1318 (2000).
- 67 Kubo T, Nishikitani Y, *J. Electrochem. Soc.* 145, 1729 (1998).
- 68 Karazhanov SZh, Zhang Y, Wang L-W, Masacarenas A, Deb S, *Phys. Rev. B* 68, 233204 (2003).
- 69 Ong, H.C.; Zhu, A.X.E.; Du, G.T.; *Appl. Phys. Lett.* 80, 941 (2002).

-
- 70 Fernández-García M, Wang X, Belver C, Iglesias-Juez A, Hanson JC, Rodriguez JA, Chem. Mater. 17, 4181 (2005).
- 71 Kang, J.; Tsunekawa, S.; Kasuya, A.; Appl. Surf. Sci. 174, 306 (2001).
- 72 Kosacki, I.; Petrovsky, V.; Anderson, H.U.; Appl. Phys. Lett. 74, 341 (1999).
- 73 Reddy, K.M.; Manorama, S.V.; Reddy, A.R.; Mater. Chem. Phys. 78, 239 (2002).
- 74 Iyer, S.S.; Xie, Y.-H.; Science 260, 40 (1993).
- 75 Mahmond, S.A.; Akl, A.A.; Kand, H.; Adbel-Had, K.; Physica B 111, 366 (2002).
- 76 Matsumoto, T.; Suzuki, J.-I.; Ohmura, M.; Kanemitsu, Y.; Masumoto Y.; Phys. Rev. B 63, 195322 (2001).
- 77 Urbach F, Phys. Rev. 92, 1324 (1953).
- 78 Melsheiner J, Ziegler D, Thin Solid Films 129, 35 (1985).
- 79 Einstein, A. Ann. Phys. Leipzig 17, 132 (1905).
- 80 Briggs, D.; Seah, M.P. *Practical Surface Analysis by Auger and X-ray Photoelectron Spectroscopy*; Wiley: New York, 1983.
- 81 Siegbahn, K.; Nordling, C.; Fahlman, A.; Nordberg, H.; Hamrin, K.; Hedman, J.; Johansson, G.; Bergmark, T.; Karlsson, S.E.; Lindgren, J.; Lindberg, B. *Electron Spectroscopy for Chemical Analysis*; Almquist and Wiksells: Stockholm, 1967.
- 82 Turner, D.W.; Baker, C.; Baker, A.D.; Brundle, C.R. *Molecular Photoelectron Spectroscopy*; Wiley: London, 1970.
- 83 Spicer, W.E. Phys. Rev. 125, 1297 (1962).
- 84 Rabalais, J.W. *Principles of Ultraviolet Photoelectron Spectroscopy*; Wiley: New York, 1977.
- 85 Hrbek, J. In *Chemical Applications of Synchrotron Radiation*; T.K. Sham, editor; World Scientific: New Jersey, 2002.
- 86 *Synchrotron Radiation, Techniques and Applications*; C. Kunz, editor; Springer-Verlag: Berlin, 1979.
- 87 Ferrer, S.; Petroff, Y. Surf. Sci. 500, 605 (2002).
- 88 Polcik, M.; Wilde, L.; Haase, J.; Brenna, B.; Cocco, D.; Comelli, G.; Paolucci, G. Phys. Rev. B, 53, 13720 (1996).
- 89 Hrbek, J.; Yang, Y.W.; Rodriguez, J.A. Surf. Sci. 296, 164 (1993).
- 90 Lee, A.F.; Wilson, K.; Middleton, R.L.; Baraldi, A.; Goldoni, A.; Paolucci, G.; Lambert, R.M. J. Am. Chem. Soc. 121, 7969 (1999).
- 91 Soriano, L.; Abbate, M.; Fernández, A.; González-Elipé, A.R.; Sirotti, F.; Rossi, G.; Sanz, J.M. Chem. Phys. Lett. 266, 184 (1997).
- 92 Smith, K.E.; Mackay, J.L.; Henrich, V.E. Phys. Rev. B, 35, 5822 (1987).
- 93 Rodriguez, J.A.; Pérez, M.; Jirsak, T.; González, L.; Maiti, A.; Larese, J.Z. J. Phys. Chem. B, 105, 5497 (2001).
- 94 Soriano, L.; Abbate, M.; Fernández, A.; González-Elipé, A.R.; Sirotti, F.; Sanz, J.M. J. Phys. Chem. B, 103, 6676 (1999).
- 95 Soriano, L.; Abbate, M.; Fernández, A.; González-Elipé, A.R.; Sirotti, F.; Rossi, G.; Sanz, J.M. Chem. Phys. Lett. 266, 184 (1997).
- 96 Soriano, L.; Abbate, M.; Fernández, A.; González-Elipé, A.R.; Sirotti, F.; Sanz, J.M. J. Phys. Chem. B, 103, 6676 (1999).
- 97 Rodriguez, J.A.; Campbell, C.T. J. Phys. Chem. B, 91, 6648 (1987).
- 98 Chaturvedi, S.; Rodriguez, J.A.; Hrbek, J. J. Phys. Chem. B, 101, 10860 (1997).
- 99 Liu, G.; Rodriguez, J.A.; Hrbek, J.; Dvorak, J.; Peden, C.H.F. J. Phys. Chem. B, 105, 7762 (2001).
- 100 Rodriguez, J.A.; Azad, S.; Wang, L.-Q.; García, J.; Etxeberria, A.; González, L. J. Chem. Phys. 118, 6562 (2003).

-
- 101 Wagner, C.D.; Riggs, W.M.; Davis, L.E.; Moulder, J.F.; Muilenberg, G.E. *Handbook of X-ray Photoelectron Spectroscopy*; Perkin-Elmer: Eden Prairie, Minnesota, 1978.
- 102 Song, Z.; Cai, T.; Chang, Z.; Liu, G.; Rodriguez, J.A.; Hrbek, J. *J. Am. Chem. Soc.* 125, 8060 (2003).
- 103 Liu, P.; Rodriguez, J.A.; Muckerman, J.T.; Hrbek, J. *Phys. Rev. B*, 67, 155416 (2003).
- 104 Egelhoff, W.G.; *Surf. Sci. Rep.* 6, 253 (1987).
- 105 Yeh, J.-J.; Lindau, I.; Sun, J.-Z.; Char, K.; Missert, N.; Kapitulnik, A.; Geballe, T.H.; Beasley, M.R. *Phys. Rev. B*, 42, 8044 (1990).
- 106 Bagus, P.S.; Pacchioni, G.; Sousa, C.; Minerva, T.; Parmigiani, F. *Chem. Phys. Lett.* 196, 641 (1992).
- 107 Wertheim, G.K. *J. Electron. Spectry.* 34, 309 (1984).
- 108 Hill, D.M.; Meyer, H.M.; Weaver, J.H. *Surf. Sci.* 225, 63 (1984).
- 109 Vazquez, R.P. *J. Electron. Spectry.* 56, 217 (1991).
- 110 Sangaletti, L.; Depero, L.E.; Bagus, P.S.; Parmigiani, F. *Chem. Phys. Lett.* 245, 463 (1995).
- 111 Bagus, P.S.; Freund, H.J.; Minerva, T.; Pacchioni, G.; Parmigiani, F. *Chem. Phys. Lett.* 251, 90 (1996).
- 112 Zhang, F.; Wang, P.; Koberstein, J.; Khalid, S. *Surf. Sci.* 563, 74 (2004).
- 113 Perebeinos, V.; Chan, S.-W.; Zhang, F. *Solid State Común.* 123, 295 (2002).
- 114 Bagus, P.S.; Pacchioni, G.; Parmigiani, F. *Chem. Phys. Lett.* 207, 569 (1993).
- 115 Hennig, D.; Ganduglia-Pirovano, M.V.; Scheffler, M. *Phys. Rev. B*, 53, 10344 (1996).
- 116 Wu, R.; Freeman, A.J. *Phys. Rev. B*, 52, 12419 (1995).
- 117 Wu, M.-C.; Truong, C.M.; Goodman, D.W. *Phys. Rev. B*, 46, 12688 (1992).
- 118 Borgohain, K.; Singh, J.B.; Rao, M.V.M.; Shripathi, T.; Mahamuni, S. *Phys. Rev. B*, 61, 11093 (2000).

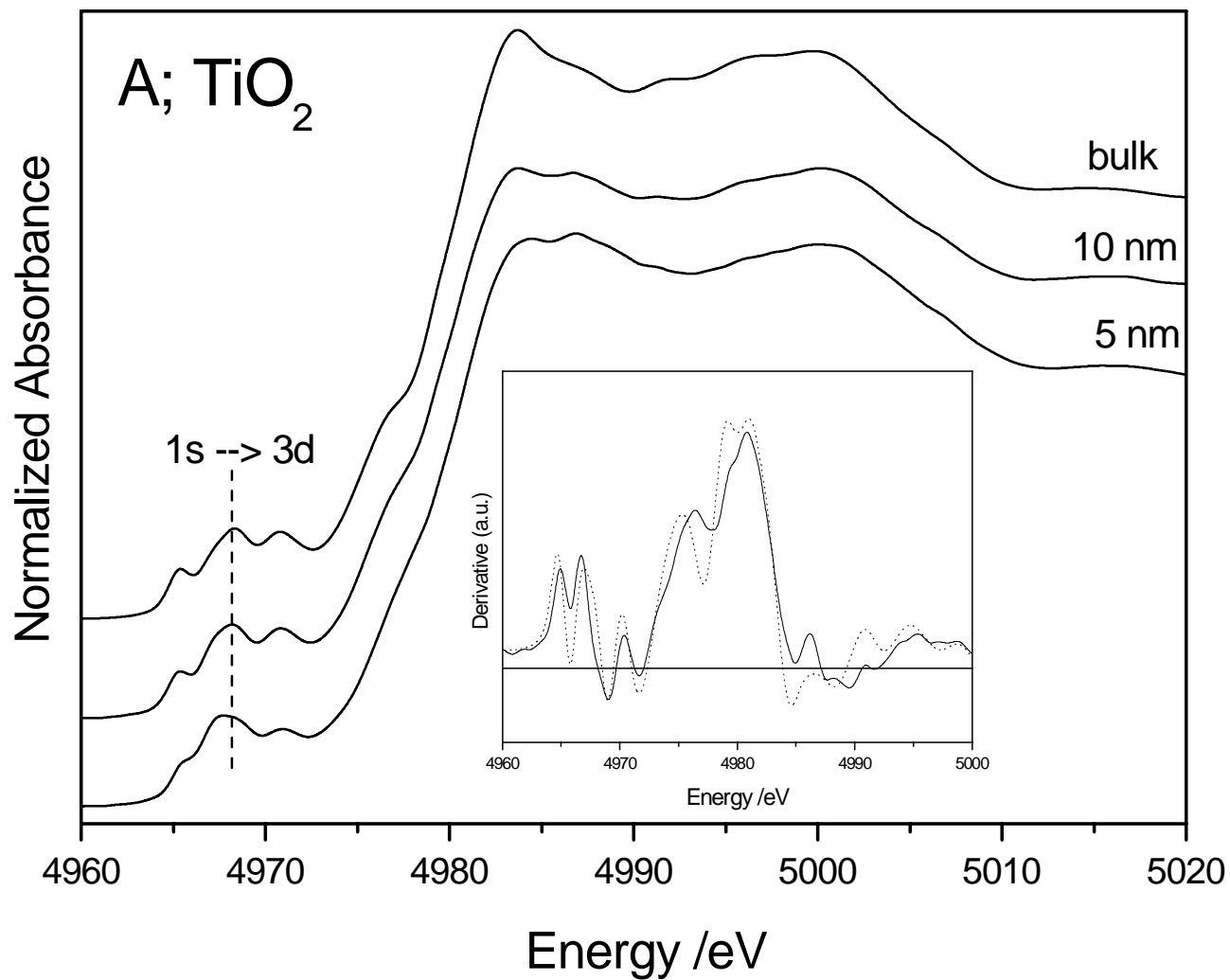


Fig 1a

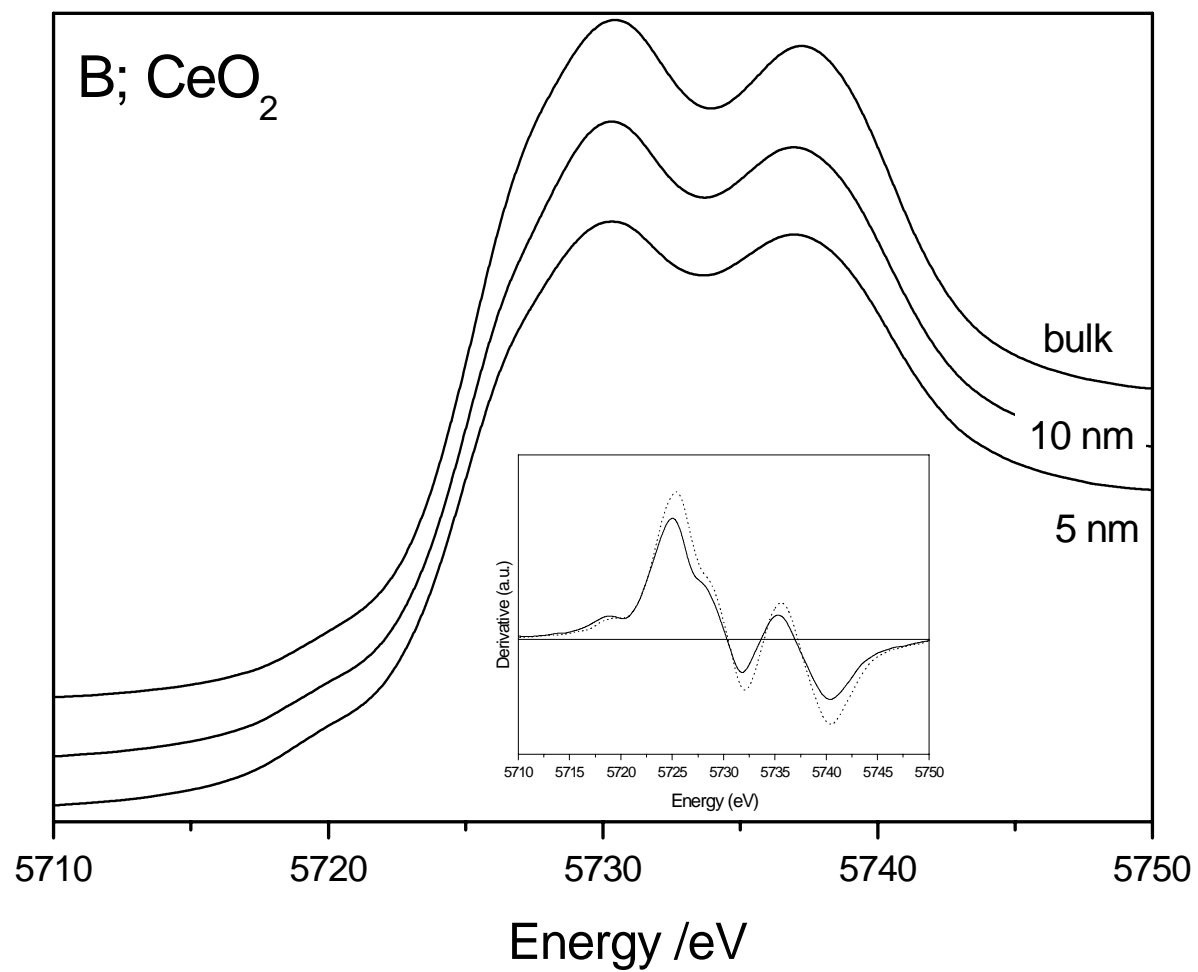


Fig 1b

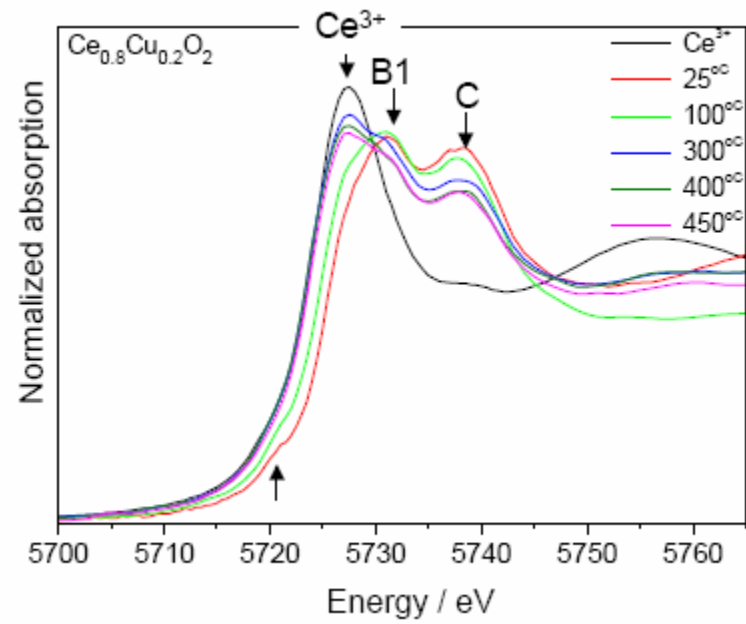
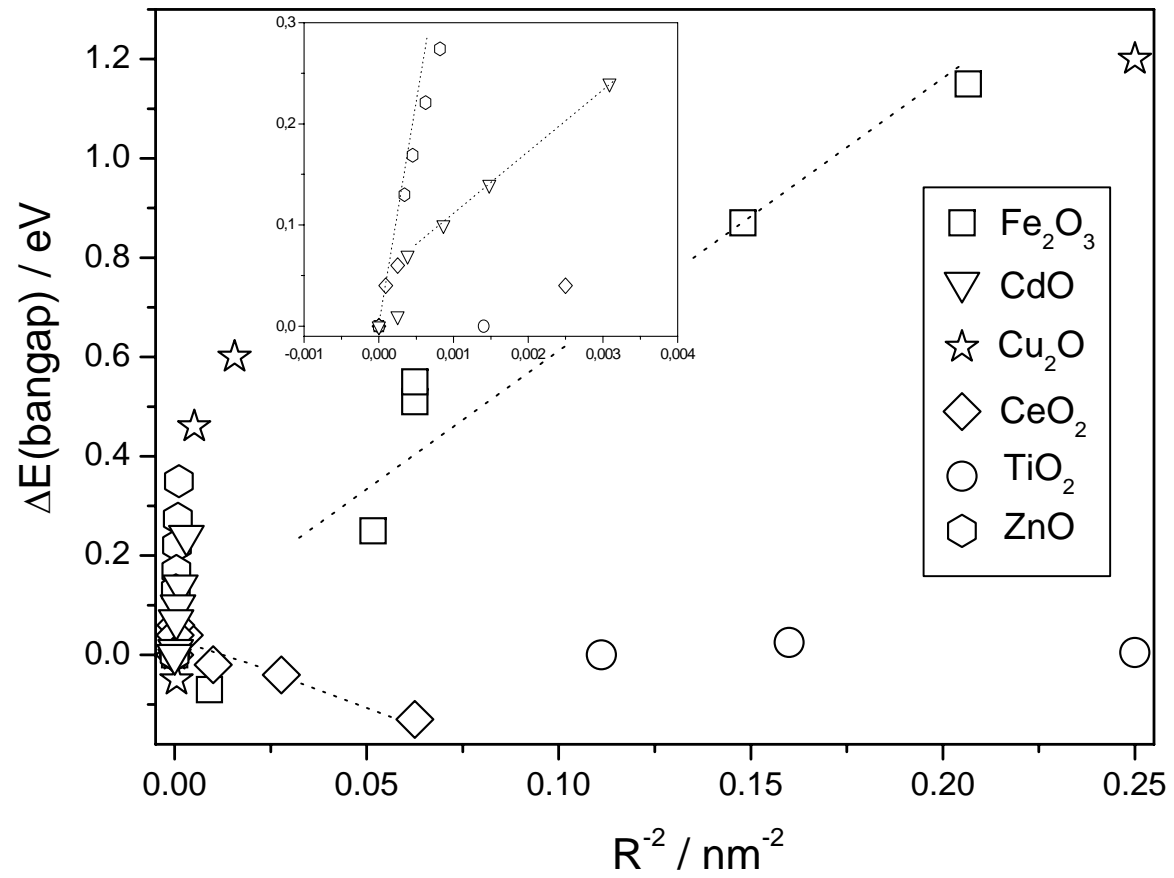


Fig 2



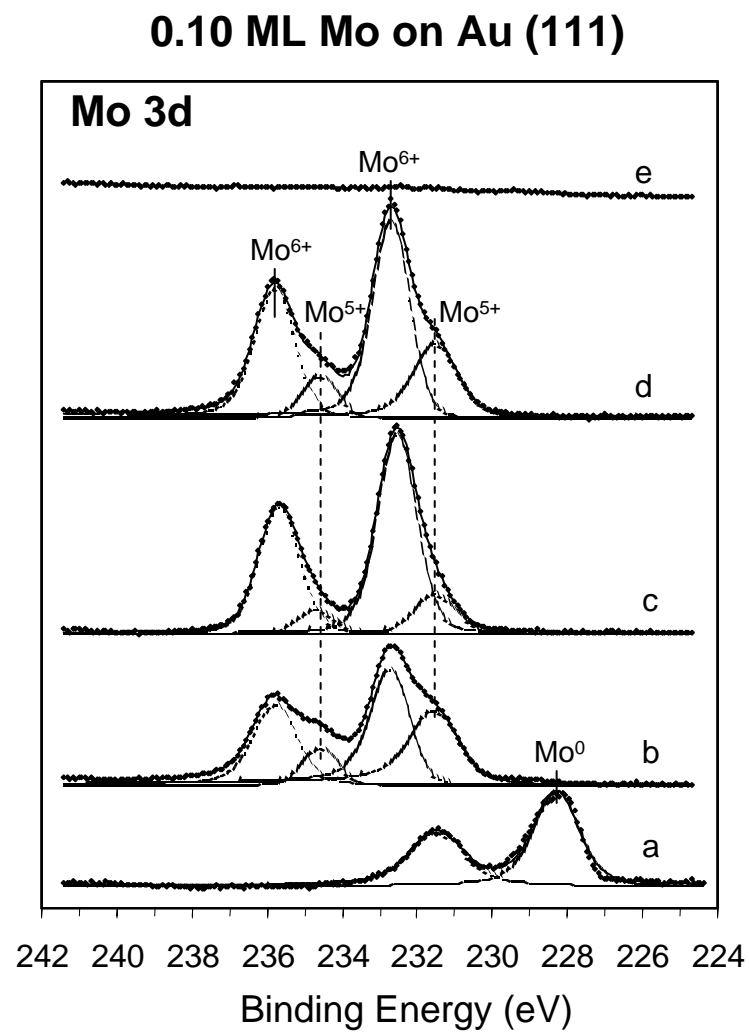
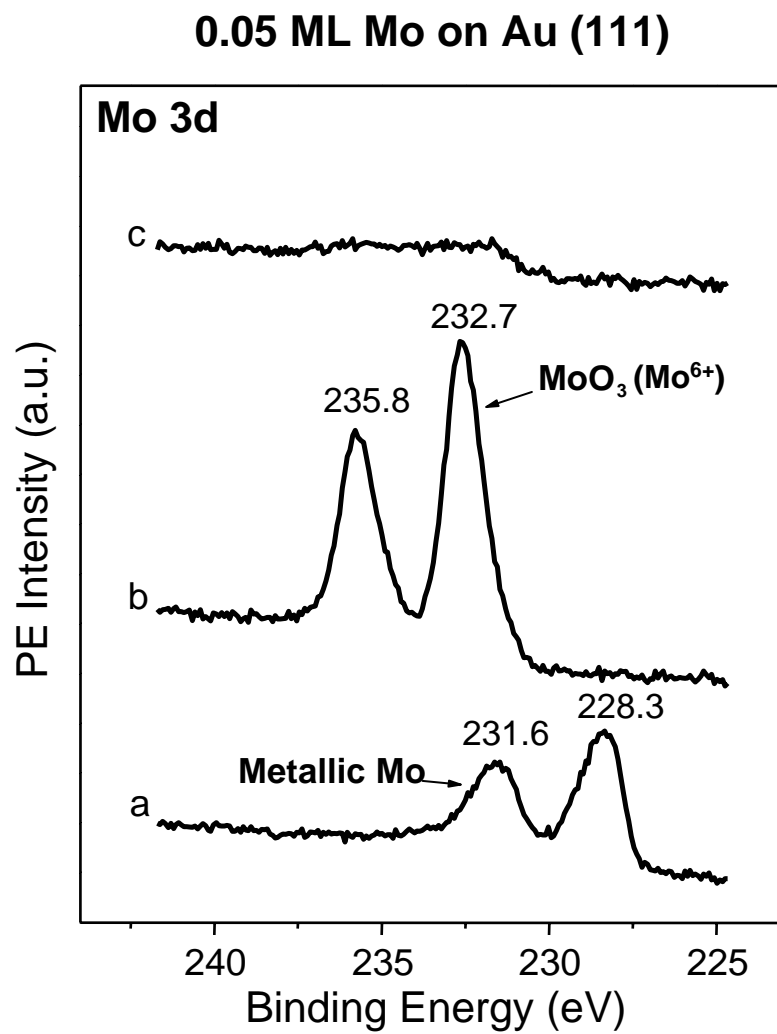


Fig. 4